Effects of eutrophication and benthic respiration on water column carbonate chemistry in a traditional hypoxic zone in the Northern Gulf of Mexico

Xinping Hu[1,*], Qian Li[2], Wei-Jen Huang[3], Baoshan Chen[4], Wei-Jun Cai[4], Nancy N. Rabalais[5], R. Eugene Turner[5]

1. Department of Physical and Environmental Sciences, Texas A&M University - Corpus Christi, Corpus Christi, Texas 78412, USA
2. State Key Laboratory of Marine Environmental Science, Xiamen University, Xiamen 3610005, China
3. Department of Oceanography, National Sun Yat-sen University, Kaohsiung 80424, Taiwan
4. School of Marine Science and Policy, University of Delaware, Newark, DE 19716, USA
5. Department of Oceanography and Coastal Sciences, Louisiana State University, Baton Rouge, Louisiana 70803, USA

* Correspondence: Xinping Hu, Xinping.Hu@tamucc.edu, 361-825-3395

Highlights

- Eutrophication dominates coastal carbonate chemistry on the Louisiana Shelf
- Benthic CO_2 contributions may further acidify hypoxic bottom water

Keywords: ocean acidification, hypoxia, northern Gulf of Mexico, dissolved oxygen.

Abstract

A simple river-ocean mixing approach has been frequently used to examine estuarine and coastal carbonate system speciation. Coastal areas receiving significant nutrient inputs, however, can have the carbonate chemistry greatly deviated from this mixing-only scheme because of disparate, but spatially coupled biogeochemical processes, i.e., intense primary production in surface waters and elevated respiration in bottom waters; the latter often leads to bottom-water hypoxia (dissolved oxygen or DO concentration < 2 mg L^{-1}) and acidification. As a result of land use change, riverine TA input is known to enhance coastal water buffer capacity, although this effect in eutrophic coastal water has not been systematically studied. The physical disturbances of shallow coastal waters by storms can disrupt bottom hypoxia through overturning the water column. This overturn has been proposed to exacerbate bottom water acidification, because of the different exchange rates of oxygen and CO_2, which could lead to a 'reset' of oxygen concentration but little change in the total dissolved inorganic carbon concentration. We used data from the summer 2010 hypoxia cruise in the northern Gulf of Mexico shelf, during which a tropical depression (Bonnie) perturbed the bottom water. Carbonate buffer capacity in both surface and subsurface waters along the salinity gradient suggested that eutrophication-induced surface production and bottom respiration far outweighed the influence of river TA variation and temperature changes in determining carbonate changes on centennial time scales. We propose, based on literature-based CO_2 flux reported in this area, that the benthic (both aerobic and anaerobic) respiration-produced CO_2 flux (with a lesser flux of alkalinity), instead of bottom water reset by storms, could be responsible for further acidifying hypoxic bottom water in addition to water column aerobic respiration.

1. Introduction

Ocean acidification (OA) is caused by the dissolution of CO_2 and subsequent dissociation of carbonic acid in seawater. As a result, decreases in both pH and carbonate saturation state (Ω) could lead to corrosive seawater conditions that are detrimental to calcareous organisms (both benthic and pelagic) (Fabry, 2008; Waldbusser et al., 2013) and fish species (Checkley et al., 2009; Cripps et al., 2011). Until recently, studies of OA mostly focused on the open ocean and tropical areas (Doney et al., 2009; Feely et al., 2004; Orr et al., 2005), where atmospheric CO_2 intrusion is the dominant acidification factor. CO_2 from both continental margin upwelling that brings up CO_2-enriched deep water (Feely et al., 2010; Feely et al., 2008) and *in situ* respiration in subsurface water column and sediment (Cai et al., 2011; Mucci et al., 2011; Wallace et al., 2014) are additional important contributing factors to coastal OA.

Some of the complexity of coastal acidification studies is a consequence of, unlike acidification in the open ocean, the freshwater input from the land from i.e., rivers (Salisbury et al., 2008) or melting glacial water (Reisdorph and Mathis, 2014). Because of vastly different freshwater end-member compositions (Pawlowicz, 2015), coastal waters all experience decrease in carbonate saturation state mostly because of lower [Ca^{2+}] in freshwater end-members than seawater (Hu and Cai, 2013; Salisbury et al., 2008), but not necessarily lower pH. For coastal oceans receiving river water with high levels of weathering products (bicarbonate), the pH can be maintained at relatively high levels in the entire salinity gradient (Hu and Cai, 2013). Estuarine and coastal waters affected by rivers with high levels of weathering products, in general, represent well-buffered systems compared to many other estuaries that have lower amounts of weathering product input. Furthermore, other than simple mixing-caused differentiation in carbonate system speciation along the salinity gradient, biogeochemical

processes (primary production and respiration) can also influence the water buffering behavior. Defining the effects of these processes on the inorganic carbon system is crucial for better understanding the response of estuarine and coastal waters to both river chemistry changes and further ocean acidification.

Recent studies have linked coastal acidification to eutrophication in multiple coastal areas, for example the northern Gulf of Mexico (nGoM) shelf (Cai et al., 2011; Sunda and Cai, 2012), the Long Island Sound (Wallace et al., 2014), and the East China Sea (Chou et al., 2013b). Excess nutrient runoff can stimulate surface algal blooms, which lead to elevated pH values and declining pCO_2 in the surface water (e.g., Chou et al., 2013a). Subsequent sinking and respiration of algal detritus and zooplankton fecal pellets will cause intense respiration in the bottom waters (Rabalais et al., 2002). Physical stratification, the same mechanism that hinders oxygen exchange between subsurface water and the atmosphere thus causes low subsurface oxygen conditions, also gives rise to a CO_2 buildup in the subsurface water, resulting in acidification (Cai et al., 2011). This same study noted a positive correlation between pH and dissolved oxygen (DO) concentration in the sub-pycnocline waters. Respiration-induced acidification, when overlaid with the gradual CO_2 buildup in the surface ocean due to atmospheric CO_2 increase, may 'amplify' the acidification signal so that the concerted impact is greater than a simple sum of changes caused by individual processes alone, which is a consequence primarily due to the non-linear response of seawater pH to CO_2 additions.

Two processes were proposed to 'counter' OA. They include increase in riverine TA flux and eutrophication-induced primary production (Borges and Gypens, 2010; Duarte et al., 2013; Nixon et al., 2015). Data for the Mississippi River indicate a long-term increase in TA input into the nGoM (Raymond and Cole, 2003; Raymond et al., 2008; Tian et al., 2015). As a result,

Duarte et al. (2013) proposed that, instead of acidification, 'basification' might actually be occurring in regions such as the nGoM. Another possible OA reduction process is TA production through anaerobic processes, such as denitrification (Fennel, 2010). Hu and Cai (2011), however, suggested that denitrification overall is not an important buffer factor tempering the amount of CO_2 increase. Instead, apparent loss of fixed nitrogen (nitrate) through biogeochemical processes leads to a net CO_2 production that outweighs the effect of TA generation, so that the overall effect is net, albeit small, acidification.

Based on the above information, it is imperative to reconcile the two seemingly conflicting ideas (i.e., acidification vs. basification) regarding how the eutrophic and hypoxic nGoM shelf, a critically important ecosystem that supports important coastal fisheries might be vulnerable to OA stress. Furthermore, the few existing studies examining the OA issue in the nGoM region focused on relatively high salinity waters (salinity>32) that are mostly of offshore origin and had relatively coarser spatial resolution (Cai et al., 2011; Wanninkhof et al., 2015), yet under hypoxic conditions (with DO level less than 2 mg L^{-1}, or 61 μmol kg^{-1} if assuming seawater density is 1.024 kg L^{-1}), lower salinity waters were also present on the nGoM shelf, especially in the shallow nearshore area. Lower salinity waters on the nGoM shelf essentially create an estuary-like condition in the nearshore region of the shelf. Therefore, a more detailed examination of freshwater influence, including excess nitrogen loading that leads to enhanced primary production and similar enhancement of bottom-water respiration under stratified conditions, on carbonate chemistry is necessary to understand ocean acidification in this eutrophic coastal system and others around the world.

We examine the distribution of Ω and pH and controlling factors on pH and water buffer capacity in the perennially-occurring hypoxic zone in the nGoM in mid-summer 2010. This area

111 has been regularly surveyed for the occurrence of hypoxia since 1985 (Rabalais et al., 2002;
112 Rabalais et al., 2001). Hurricane Alex crossed the mid-Gulf in early July 2010 and made landfall
113 near the US-Mexico border (Pasch, 2010). Shortly afterwards, the Tropical Depression Bonnie
114 briefly formed outside of the nGoM and dissipated near the Mississippi River delta on July 26th
115 (Wang and Roberts, 2013), overlapping two days with the cruise. The later storm altered the
116 usual route of the hypoxia survey such that the sampling started mid-shelf off the Atchafalaya
117 River delta towards the Texas-Louisiana Border and then eastward to the Mississippi River delta
118 as opposed to the planned east to west direction (Fig. 1a). We identified well-oxygenated waters
119 in the mid-shelf of the nGoM as a result of the storm. These conditions offered an opportunity to
120 examine how the hypoxic shelf water carbonate system responded to storm activities.

121 **2. Materials and Methods**

122 2.1. Sampling locations

123 The cruise for hypoxia determination occurred during July 24-31, 2010 and covered the area
124 from the Southwest Pass of the Mississippi to 94.5°W, well onto the Texas shelf, in water depths
125 of <10 m to the 50-m isobaths (see sampling stations in Fig. 1). The study area has frequent
126 occurrence of summer hypoxia (Rabalais et al., 2007; Rabalais et al., 2001). A total of 58
127 stations ranging from 5.6 m to 48.9 m water depth were sampled for surface and bottom waters.

128 2.2. Sample collection and analyses

129 Seawater samples were all taken using 5-L Niskin bottles on a CTD-rosette frame from both
130 the surface (~0.5 m depth) and bottom (~0.5 m above the seafloor) waters. We followed the
131 protocols outlined in Dickson et al. (2007) to collect water samples using 250-mL ground neck
132 borosiliate glass bottles. Saturated $HgCl_2$ (100 μL) was added into each sample as a preservative.
133 All samples were kept refrigerated at 4°C in the dark until analysis, within one month of the

sample collection. Nutrient samples were collected from surface water (bucket) and near bottom (within 0.5 m of the bottom) and frozen until analysis.

The concentrations of total alkalinity (TA) and total dissolved inorganic carbon (DIC) were determined using Gran titration on an alkalinity titrator (Apollo Scitech Inc.) and infrared detection for acid-stripping CO_2 on a DIC analyzer (Apollo Scitech Inc.) (Chen et al., 2015), respectively. Certified reference materials (CRM) obtained from Dr. A. Dickson's lab at the Scripps Institution of Oceanography were used to calibrate and ensure the performance of both the alkalinity titrator and DIC analyzer. Analytical precisions for both TA and DIC analyses were both ± 0.1% or better. We also used unpurified m-cresol purple (mCP, Acros®) to measure pH at 25°C in a water-jacketed flow cell on a Shimadzu UV-1601 spectrometer with the experimental setup similar to that in Carter et al. (2013). The equation in Clayton and Byrne (1993) was used to calculate the pH values. Although given the unknown impurity that may existed in the reagent (Liu et al., 2011), these data were only useful for evaluating our analytical precision (see Section 3.1 for details). Unfiltered samples were analyzed for DIN (ammonium, nitrate, and nitrite), orthophosphate (DIP), and silicate following EPA methodology (353.2, 350.1, and 365.2, in USEPA, 1993) using a Lachat auto-analyzer II system (8000 series) equipped with an autosampler (ASX-400 series). Dissolved oxygen concentration was measured using a YSI 6820 meter calibrated against Winkler titrations for dissolved oxygen. Oxygen concentrations from the YSI 6820 were recalculated as necessary based on the Winkler-determined dissolved oxygen concentrations.

2.3. Carbonate system speciation calculations

We evaluated the dynamics of the carbonate system and its association with environmental factors, by choosing measured TA and DIC as the input pair as well as nutrients (silicate,

157 phosphate) for the carbonate system speciation calculations based on the assumption that
158 contribution of organic alkalinity is negligible in the nGoM shelf waters (Guo et al., 2012; Yang
159 et al., 2015) (see Section 3.1 for a detailed discussion). Here the $\Omega_{aragonite}$ (carbonate saturation
160 state with respect to aragonite), pH_T (pH on total scale), and pCO_2 values were all calculated for
161 *in situ* conditions. K_1 and K_2 values from Millero (2010) were used in the calculation because
162 they cover the widest salinity range (1-50) and the lowest salinity was 6.9 in our sampled waters.
163 For calcium concentration, we took the average value (1.07±0.18 mmol kg^{-1}) of four biweekly
164 measurements (5/5/2010-6/16/2010, USGS, http://nwis.waterdata.usgs.gov/usa/nwis/qwdata) to
165 represent the freshwater end-member and the standard 10.28 mmol kg^{-1} at salinity 35 as the
166 oceanic end-member that was built-in in the program CO2SYS (Pierrot et al., 2006). $\Omega_{aragonite}$
167 values calculated directly from the MatLab version CO2SYS program (V1.1) were corrected
168 using the river-ocean $[Ca^{2+}]$-salinity linear relationship. This correction was required as the
169 results from CO2SYS calculation alone could significantly underestimate $\Omega_{aragonite}$ in low salinity
170 samples, for example, a 10% underestimation would occur for the bottom water with the lowest
171 salinity (S=18.1).
172 2.4. Buffer factor
173 The buffer of seawater against CO_2 addition ($ß_{DIC}$) is defined in the following equation
174 (Egleston et al., 2010) after a correction to a sign error in the original version (J. Orr, personal
175 comm.). The calculation was done using the R software package SeaCarb (Gattuso et al., 2016).
176 $$ß_{DIC} = (\partial \ln[H^+]/\partial DIC)^{-1} \quad (1)$$
177 Essentially, $ß_{DIC}$ is a function of carbonate alkalinity, total dissolved DIC, pH, and borate
178 chemistry, and is also affected by salinity and temperature (through their control on acid-base
179 equilibria of both the CO_2 system and the borate system).

3. Results

3.1. Carbonate system internal consistency

Manufacturer supplied reagents were used extensively in oceanographic studies (Clayton and Byrne, 1993; Mosley et al., 2004) before the formal adoption of purified pH-sensitive dyes (Liu et al., 2011; Yao et al., 2007). Even though purity-related biases in the obtained pH values were unknown, it was still worth using this pH dataset to cross-examine TA and DIC data for quality assurance purposes. Because the equation for pH calculation in Clayton and Byrne (1993) only applies to salinity 30-37, we chose to use salinity > 30 waters only for this comparison (maximum observed salinity on this cruise was 36.1). Both Chen et al. (2015) and Patsavas et al. (2015) recommend using the carbonic acid dissociation constants (K_1 and K_2) from either Lueker et al. (2000) or the refit values (Dickson and Millero, 1987) based on the study by Mehrbach et al. (1973) for internal consistency check. More recently, Chou et al. (2016) suggested that using K_1 and K_2 values from Millero et al. (2002) generates the best agreement between calculated and measured TA values. We first used carbonate dissociation constants K_1 and K_2 in Lueker et al. (2000), the dissociation constant of bisulfate in Dickson et al. (1990), and the total boron concentration in Uppström (1974), to calculate TA based pH and DIC. ΔTA (i.e., the difference between measured and calculated TA) was 12.9±7.8 μmol kg^{-1} (N=94); if only salinity 30-35 waters were considered, then the ΔTA was 12.5±7.5 μmol kg^{-1} (N=73). The two sets of residuals were not significantly different from each other (two-tailed t test, p=0.82). For the dissociation constants in Mehrbach et al. (1973) that were refitted by Dickson and Millero (1987), essentially the same ΔTA values were obtained compared to using the Luerker et al. (2000) constants (differ by 0.2-0.3 μmol kg^{-1}). If the K_1 and K_2 values in Millero (2010) were used, then the ΔTA for both salinity > 30 and 30-35 waters increased slightly to 14.6±7.8 and 14.3±7.6 μmol kg^{-1},

203 respectively. Finally, using the K_1 and K_2 values in Millero et al. (2002) resulted in ΔTA of
204 12.3±7.5 and 10.5±7.6 µmol kg^{-1} for salinity > 30 and 30-35 waters, respectively. Even though
205 the difference between the measured and calculated TA appeared fortuitously close to the
206 estimated organic base concentration (~13 µmol kg^{-1}) in coastal waters with salinity <35
207 (Patsavas et al., 2015), we doubt that there was a significant organic alkalinity contribution to
208 this coastal ocean because a previous study suggested that the organic alkalinity is negligible in
209 the Mississippi Rivers waters and downstream coastal nGoM (Guo et al., 2012). Yang et al.
210 (2015) recently examined the organic alkalinity issue in the nGoM shelf waters and found that
211 the difference between TA calculated using DIC and pH_T (but based on purified mCP and an
212 updated equation in Liu et al. (2011)) and measured TA is essentially zero (0.1-1.0 µmol kg^{-1}),
213 which corroborates the findings of Guo et al. (2012). It is likely, therefore, that our measured pH
214 values were slightly biased toward lower values (by ~0.054), which is similar to the observation
215 in Liu et al. (2011) who concluded that using unpurified mCP would generate slightly lower pH
216 values compared to using the purified one. Nevertheless, our analytical precision and data quality
217 as represented by the variance of the residuals (ΔTA, ±7-8 µmol kg^{-1}) was similar to those
218 (±(3.45-7.37) µmol kg^{-1}) obtained in larger scale coastal studies along the U.S. coasts (Patsavas
219 et al., 2015).

220 3.2. Salinity, Ω_{arag}, pH and DO distributions

221 The surface waters had moderate to high $\Omega_{aragonite}$ and pH_T values (3.9-8.1 and 8.04-8.47,
222 respectively, Fig. 1). Higher $\Omega_{aragonite}$ and pH_T coincided with lower salinity nearshore surface
223 waters or river plume waters (Fig. 1b, c). The higher salinity surface waters, as represented by a
224 'core' in water depth ≥20 m at 92-93°W (salinity ~34.1, Fig. 1a), had the lowest $\Omega_{aragonite}$ and
225 pH_T values.

226 Compared to the more gradual transitions of these parameters in the surface, bottom water
227 $\Omega_{aragonite}$ and pH_T exhibited rather patchy distributions. Moderate to high $\Omega_{aragonite}$ and pH_T values
228 were observed (Fig. 1 f, g) at the few shallow water stations. For example, values up to 5.9 for
229 $\Omega_{aragonite}$ and 8.30 for pH_T were observed in the bottom waters near the mouth of the Atchafalaya
230 Bay, and values of 6.2 ($\Omega_{aragonite}$) and 8.34 (pH_T) were observed in the nearshore stations close to
231 the Louisiana-Texas border (Fig. 1 e, f). In addition, 'pockets' of low and high Ω and pH waters
232 appeared alternately west of 91°W, with the lowest Ω (1.63) and pH_T (7.6) values found within
233 the 20-m isobath close to the Louisiana-Texas border.
234 The bottom water DO concentrations (Fig. 1 h) essentially followed the $\Omega_{aragonite}$ and pH
235 distributions (Fig. 1 f, g). Spatial discontinuity in DO concentration was observed across the
236 surveyed area likely due to the storm activity. A few pockets of low DO waters appeared at 93-
237 94°W, near 92°W, and from the mouth of Terrebonne Bay to the Mississippi River delta
238 Southwest Pass (Fig. 1h), with most of low DO values areas falling within the 20-m isobath. The
239 lowest bottom DO concentration (11.1 μmol kg^{-1}) observed during the 2010 sampling period
240 (Fig. 1 h) corresponded to the lowest pH_T and $\Omega_{aragonite}$ values found west of our study area. In
241 contrast, two pockets of higher DO waters (up to ~170 μmol kg^{-1}) were observed in mid-shelf in
242 20-50 m water depth.
243 3.3. Buffer factor – surface and bottom comparison
244 In current seawater carbonate conditions, higher $ß_{DIC}$ value indicates greater buffer capacity
245 in the seawater. A comparison between the surface and bottom waters (Fig. 2) indicated higher
246 buffer capacity in surface water in general, especially in the lower salinity nearshore waters
247 (except in a small area next to the mouth of the Mississippi River where river water dominated).

248 The bottom water $ß_{DIC}$ exhibited a similar pattern as those of Ω, pH_T, and DO with overall lower
249 values than the surface water (Fig. 1).

250 **4. Discussion**

251 4.1. Biogeochemical reaction-induced pH deviations from conservative mixing

252 Eutrophic estuarine and coastal environments are known to have highly productive surface
253 waters that can have both depressed pCO_2 and elevated pH (Borges and Gypens, 2010; Chou et
254 al., 2009; Guo et al., 2012; Hagens et al., 2015; Huang et al., 2015; Nixon et al., 2015; Zhai et
255 al., 2007). In fact, in the Mississippi River plume area, pH has been observed to reach 8.4-8.5 (on
256 total scale) in summer, and the pH in the river plume can be maintained at high levels (>8)
257 throughout an annual cycle (Guo et al., 2012). Similarly, the high pH waters (>8.4) were
258 observed during the cruise in surface waters near freshwater inflows where salinity ranged from
259 16 to 25.

260 In a previous study, Hu and Cai (2013) used a conservative mixing scheme to examine
261 carbonate system speciation in estuarine waters, including the 'salt-wedge' type Mississippi
262 estuary that is formed by lower salinity river discharge sitting on top of higher salinity offshore
263 ocean water. Here we considered more realistic scenarios that included both primary production
264 (in surface) and respiration (bottom), to examine factors that contributed to pH dynamics in these
265 highly heterogeneous shelf waters.

266 Both the Atchafalaya and Mississippi rivers had essentially the same TA levels during May-
267 July 2010 (2460±393 µmol kg^{-1} and 2450±487 µmol kg^{-1}, respectively
268 (http://nwis.waterdata.usgs.gov/nwis/qwdata). The total nitrate+nitrite (NO_x) concentrations
269 during the same period were 125±30 µmol kg^{-1} and 98±7 µmol kg^{-1} in the Mississippi and the
270 Atchafalaya rivers, respectively. We used the discharge ratio of 4.2:1 between the Mississippi

271 and Atchafalaya rivers observed in this period to form a 'composite' NO_x concentration of 120
272 µmol kg^{-1}. River DIC concentrations were calculated using the two extreme TA values (1940
273 µmol kg^{-1} and 2960 µmol kg^{-1}, USGS) observed during the May-July period in 2010 and a fixed
274 pCO_2 of 1000 µatm (Guo et al., 2012). For the seawater end-member, we chose the TA-salinity
275 relationship of the surface Atlantic Ocean (Millero et al., 1998) to calculate TA at the observed
276 maximum salinity 36.1; we then took atmospheric CO_2 dry fraction (xCO_2) value in 2010 (390
277 ppm, https://www.esrl.noaa.gov/gmd/ccgg/trends/) to calculate pCO_2 using salinity in
278 conjunction with both average surface temperatures (30.6°C) and that of the deepest water
279 (20.8°C, 47 m) found during this cruise (Weiss, 1974), assuming air-sea CO_2 equilibration at
280 both temperature conditions. DIC concentrations at the two temperatures were calculated using
281 TA and pCO_2. The conservative mixing line (the solid line in Fig. 3) reflects the average values
282 of four river and ocean endmember mixing conditions (high vs. low river TA and high vs. low
283 seawater temperature) with the shaded area representing one standard deviation of the average of
284 the four mixing curves. The same endmember and temperature conditions were used to obtain
285 the following hypothetical reaction/mixing lines for both complete NO_x use through
286 photosynthesis and complete DO consumption (i.e., anoxia). Briefly, assuming that all NO_x
287 along the salinity gradient was consumed by phytoplankton (seawater end-member had zero
288 concentration) following the Redfield stoichiometry (Huang et al., 2012), then an idealized pH
289 distribution along the salinity gradient (the dotted line in Fig. 3) is expected. For the anoxic
290 condition, we assumed oxygen was depleted from saturated levels along the salinity gradient,
291 and that the DIC and nutrient release also followed Redfield stoichiometry (the dashed line in
292 Fig. 3). Clearly, the extremely variable pH in these shelf waters significantly deviated from what
293 the conservative mixing would predict (the solid line in Fig. 3), with the surface water being

294 significantly above the mixing line except at high salinity end (>33) due to photosynthesis and
295 the pH in bottom waters significantly below the mixing line due to respiration. Nevertheless, the
296 pH values were bracketed by these two extreme scenarios (i.e., complete nutrient utilization and
297 complete water column O_2 consumption).

298 4.2. Relative importance of nutrient utilization and river water TA on coastal water buffer
299 capacity

300 The buffer factor $ß_{DIC}$ can be used to evaluate the response of seawater pH to CO_2 addition
301 via different processes (respiration or anthropogenic CO_2 intrusion). The range of $ß_{DIC}$ spanned
302 from 0.16 to 0.36 mmol kg^{-1} (Fig. 2). By comparison, the entire global surface ocean had a $ß_{DIC}$
303 range of ~0.16-0.28 mmol kg^{-1} as of 1994 (the value decreases with increasing atmospheric CO_2
304 uptake) (see a global synthesis in Egleston et al., 2010). Understandably, the surface waters in
305 the nGoM became rather 'basified' due to its much elevated buffer capacity than being acidified
306 in the open ocean caused solely by anthropogenic CO_2 intrusion (Duarte et al., 2013).

307 Three factors contributed to elevated buffer capacity in the nGoM hypoxic zone: 1) the
308 presence of highly buffered river water (high TA), 2) relatively warm temperature, and 3) high
309 surface primary productivity because of high riverine nutrient input. Hu and Cai (2013) showed
310 that, when comparing the two large river-influenced estuaries (e.g., Amazon and Mississippi),
311 the simulation of a simple mixing indicates that the $ß_{DIC}$ in the Mississippi River estuary is
312 consistently higher throughout most of the salinity range except in the high salinity region (>31).
313 The difference in buffer capacity in high salinity waters is caused by a difference in the carbonic
314 acid dissociation constants because of temperature difference (the Amazon estuary has higher
315 temperatures). In lower salinity waters however, the difference in $ß_{DIC}$ is caused by the difference
316 in river end-member carbonate chemistry, i.e., the Mississippi River has high levels of

317 weathering products. For example, average TA over the past 20 years was greater than 2200
318 µmol kg^{-1} (USGS) yet pCO_2 levels are moderate (~1000 µatm, Guo et al., 2012). Thus this river
319 is well buffered. In contrast, the Amazon River has much lower TA levels (in the range of 300-
320 400 µmol kg-1, e.g., Cooley, 2006) yet higher pCO_2 (2500-5000 µatm) (Abril et al., 2015; Devol
321 and Hedges, 2001).

322 We used the varying river end-member TA values (1940 µmol kg^{-1} and 2960 µmol kg^{-1},
323 USGS) and surface and bottom temperatures (30.6°C and 20.8°C), to calculated $ß_{DIC}$ values
324 based on conservative mixing between river and ocean waters (Fig. 4). Clearly, both higher river
325 TA level and higher temperature could increase $ß_{DIC}$ throughout the salinity gradient. The
326 magnitude of $ß_{DIC}$ increase caused by river TA increase was very small. For example, a 52%
327 increase from 1940 µmol kg^{-1} to 2960 µmol kg^{-1} only increased $ß_{DIC}$ by up to 0.03 mmol kg^{-1} in
328 both surface and bottom waters, and this TA increase would correspond to the magnitude of net
329 increase in Mississippi River TA in the last 50-100 years (Raymond and Cole, 2003; Raymond et
330 al., 2008). Buffer factor increase due to river end-member change would diminish to zero at the
331 seawater end-member as river influence disappears. Similarly, a difference of 10°C resulted in a
332 $ß_{DIC}$ difference of up to 0.04 mmol kg^{-1} for both river TA end-member conditions, thus the $ß_{DIC}$
333 increase caused by climate change (i.e., targeted 2°C increase within this century, IPCC, 2013)
334 would be much smaller than the changes to $ß_{DIC}$ caused by this 10°C change.

335 The $ß_{DIC}$ in all surface and a small number of bottom water samples (from shallow depth)
336 exceeded what the simple mixing lines would predict, and the change can be up to a 0.13 mmol
337 kg^{-1} increase in surface water and 0.07 mmol kg^{-1} decrease in bottom water compared to the
338 conservative mixing scenario (Fig. 4). This is a similar result as the deviation of pH from
339 conservative mixing (Fig. 3). Clearly, surface productive water in the mid-salinity range (16-25)

had the highest buffering capacity against a CO_2 addition. Conversely, the bottom waters had much depressed $ß_{DIC}$ values compared to the mixing lines, indicating a greatly weakened buffer capacity against CO_2 addition, which explains why the hypoxic (and low pH) bottom water would have larger pH response (i.e., more pH decrease) to a given amount of CO_2 addition than the highly buffered surface water (Cai et al., 2011).

It is clear that the eutrophication-induced buffering capacity change in coastal waters is much greater than either the river water composition change or temperature increase, and that the biological enhancement in surface waters and depression in bottom waters of buffer capacity remains the dominant factor controlling the coastal carbonate system as long as significant nutrient reduction is not achieved.

4.3. Disturbance to the carbonate system caused by storm activities and benthic CO_2 contribution to acidification

During the 2010 summer hypoxia cruise, the passage of a tropical depression Bonnie in this region offered an excellent opportunity for us to examine the physical disturbances to the CO_2 system in these shallow coastal waters. Because the vertical stratification is an important prerequisite for coastal hypoxia formation, the tropical storms and depression facilitated vertical mixing and disrupted bottom water hypoxia (Rabalais et al., 2010; Rabalais et al., 2007). Such physical disturbance also resulted in a smaller hypoxic area in 2010 than that predicted based on riverine nutrient loading (Turner et al., 2006), because most of the hypoxic areas lie within the 50-m isobath and are relatively easily influenced by large scale weather conditions such as the tropical depression. Similarly, water column overturning likely disrupted the otherwise widespread low pH and Ω conditions in the bottom water by introducing higher pH (low pCO_2) and oxygen-rich surface waters into the bottom via mixing (Figs. 1, 2, and 6). We suspect that

363 overturning of the subsurface CO_2-rich water could be the reason for observed elevated pCO_2
364 levels (up to 427 µatm, vs. ~379 µatm in the atmosphere), but near ~100% DO at 92-94°W that
365 was south of the 20 m isobath (Fig. 5a).

366 Cai et al. (2011) studied the pH and oxygen relationship in both the nGoM and East China
367 Sea and found that low DO bottom waters had low pH values and these pH values deviated from
368 what the multiyear pH-DO relationship might suggest. These authors attributed this observation
369 to different air-sea exchange rates of CO_2 and oxygen following storm-caused water column
370 overturning (oxygen exchange is faster, Williams and Follows, 2011). The re-establishment of
371 hypoxic condition from the DO-'reset' bottom waters, along with minimal change in DIC
372 following storm activities, could acidify the subsurface water even more.

373 If we use the same criteria (i.e., >12 m water depth and salinity > 32) and overlay the 2010
374 bottom water data onto the same nGoM dataset reported in Cai et al. (2011), the DO and pH
375 values from the area with maximum DO concentration in mid-shelf (28.7-28.9°N, 92.0-92.5°W)
376 agreed well with the multiyear observations (Fig. 6a). Note that the Fig. 2 in Cai et al. (2011)
377 inadvertently included deeper waters (>50 m) from their July 2009 cruise, which resulted in
378 lower pH values in high DO section of their figure, and these data were excluded here (Fig. 6a).
379 If differential gas exchange between CO_2 and O_2 occurred to a significant extent, then one might
380 expect a lower pH at the area of re-aeration to begin with. Hypothetically, if we allow the few
381 locations with high bottom DO (~170 µmol kg^{-1}) 'reset' water to experience aerobic respiration
382 following the Redfield stoichiometry (Xue et al., 2015), then lower DO waters would follow the
383 calculated pH evolution curve (the solid black and gray lines in Fig. 6a). Some actual pH values
384 at low DO conditions, however, were still 0.06-0.07 pH units lower than the predictions at their
385 respective DO concentrations (Fig. 6a). Similarly, bottom water DIC concentration also appeared

386 to deviate from the expected Redfield reaction stoichiometry (the solid black and gray lines in
387 Fig. 6b), i.e., excess DIC 'enrichment' occurred along with DO consumption. We explain this
388 discrepancy by proposing that these additional pH decreases were caused by a benthic DIC
389 contribution.

390 It is well known that anaerobic respiration in suboxic and anoxic nearshore sediments could
391 dominate benthic respiration because oxygen can be depleted quickly within a few millimeters of
392 the surface sediments (Canfield et al., 1993). Previous studies, using different techniques
393 (benthic chamber and ship-board incubations) in the nGoM shelf sediments, suggested that
394 benthic sediment community oxygen consumption is less than one half of DIC flux under
395 hypoxic conditions, with the rest of DIC production attributed to sulfate reduction and
396 denitrification (Lehrter et al., 2012; Rowe et al., 2002). Because the seawater CO_2 system is
397 influenced by relative TA and DIC changes, the higher DIC input rate than TA ($\Delta TA/\Delta DIC<1$)
398 could cause acidification (bottom water TA and DIC concentration ratio in our studied region
399 ranged from 1.07 to 1.18). Hu and Cai (2011) compiled sediment TA and DIC fluxes across the
400 global ocean and found that the TA/DIC flux ratios never exceeds 1 (with an average at ~0.5)
401 within the 100-m water depth. Note that a global modeling effort (Krumins et al., 2013) indicated
402 that the net benthic TA flux (after correcting for re-oxidation of reduced species) to DIC ratio is
403 only 0.23. Even though there are no simultaneously measured TA and DIC fluxes in nGoM, it is
404 likely that this 'excess' benthic DIC (compared to TA) supplied through benthic processes could
405 contribute to further pH decrease compared with the projected water column pH decline induced
406 by respiration only, which starts from the re-aerated bottom water. This benthic DIC production
407 is decoupled from oxygen consumption, as the Redfield stoichiometry would suggest.

In fact, despite years of study, the issue regarding the role of sediment in hypoxia formation is still unresolved. Some studies suggested that water column dominates oxygen consumption (e.g., McCarthy et al., 2013; Murrell and Lehrter, 2011), while others indicated otherwise with high benthic consumptions (e.g., Eldridge and Morse, 2008). Nevertheless, the benthic DIC contribution originating from anaerobic respiration has not been considered in bottom water acidification in the literature. Given the relatively thin benthic hypoxic layer (from less than 1 m to several meters), the benthic DIC contribution could play an important role in controlling the bottom water CO_2 system. We used summer benthic DIC flux values (24-55 mmol m^2 d^{-1}) measured in August, 1994 by Rowe et al. (2002) and assumed that half of this benthic DIC flux was from anaerobic respiration, with the other half going through aerobic respiration that can be integrated with water column respiration, and the hypoxic layer of 3.9 m thick (Boucher et al., 1994), and computed a DIC accumulation rate of 3-7 µmol kg^{-1} d^{-1} in bottom water. If we further assume that the benthic TA flux is 1/4 of total benthic DIC flux (Krumins et al., 2013), then the TA accumulation rate would be 1.5-3.5 µmol kg^{-1} d^{-1}. Due to rapid oxygen consumption, generally bottom waters can reach zero oxygen in less than four weeks, and it may take as little as one week to form anoxia (Rabalais et al., 2007). Assuming that it took the relatively DO-'reset' bottom water (~170 µmol kg^{-1}) three weeks to reach oxygen-free condition in our case, the benthic processes could add 68-155 µmol kg^{-1} DIC and 34-78 µmol kg^{-1} TA into the bottom water, respectively. As a result of both water column and benthic processes, the bottom water pH_T would decrease an additional 0.08-0.20 pH units compared to aerobic respiration alone. Benthic DIC flux values reported by Lehrter et al. (2012) are comparable to the lower bound in Rowe et al. (2002), thus an additional pH reduction of ~0.08 would still be expected if using their measured value. Therefore, it is likely that the benthic DIC production, instead of the

different gas exchange rates during water column overturning caused by storm events, could be a sufficient cause for further pH drawdown in the hypoxic waters. Here mineral acid production due to the oxidation of reduced species in sediment pore waters (metals, ammonia, and reduce sulfur) was not accounted for, although this acid production is even capable of dissolving sedimentary carbonate (e.g., Green and Aller, 1998). Thus further evaluation of pH decrease in very low oxygen bottom water is needed.

The benthic-pelagic coupling integrating both water column processes and sediment fluxes would be useful to fully determine the carbonate chemistry changes in stratified shallow waters. Further, the benthic DIC contribution and other acid production may not only be of importance to the nGoM bottom waters, but in all other shallow hypoxic systems with stagnant bottom water layers, where metabolic products buildup is allowed.

5. Conclusions

The coastal ocean carbonate system is controlled by many physical and biogeochemical processes that range from river-ocean mixing, air-sea exchange, primary production, and respiration. The eutrophication-led intensive surface production and strong near bottom respiration coexist in a very confined geographical area within a few meters or less water depth. Therefore, a simple examination of carbonate chemistry based on physical mixing alone (i.e., Hu and Cai, 2013) cannot adequately address how the carbonate system behaves along a salinity gradient in the coastal ocean. Deviations from ideal mixing in both surface and subsurface waters are especially important in eutrophic systems such as the nGoM. We found extremely basic conditions in surface water and acidified bottom water situations in the wide buffer range greater than that in the global surface ocean. Furthermore, the eutrophication-induced surface production

453 and below the pycnocline aerobic respiration dominated carbonate equilibrium and far
454 outweighed river TA variation and expected temperature changes on a century time scale.
455 Physical disturbances (wind, storms) can aerate shallow coastal ocean and disrupt low
456 bottom water hypoxia. The vertical mixing caused by storm activities will also alleviate bottom
457 acidification and 'reset' the system. However, our observed pH and DO relationship at low
458 oxygen conditions still deviated from what aerobic respiration of this reset water column would
459 predict. To explain this discrepancy, we propose that benthic DIC contribution of an anaerobic
460 origin, in addition to aerobic respiration, contributed to this excess acidification. This benthic
461 flux may be important for carbonate speciation in other shelf areas, as most shelf sediment has
462 lower TA/DIC flux ratios (much less than 1) than the water column values (typically greater than
463 1).
464

Acknowledgements

This study was funded by grants from the Gulf of Mexico Research Initiative RFP-III and RFP-II (GOMRI-II-020). The cruise was funded by NOAA, Center for Sponsored Coastal Ocean Research Grant No. NA09NOS4780204. We thank G. Han for helping with the DIC analysis, and the crew of the R/V *Pelican* and the research scientific team for successful collection of data. Two anonymous reviewers and the Associate Editor Dr. Benitez-Nelson provided constructive comments that helped to improve the quality of this work. XH dedicates this study to his friend and former colleague - Dr. Yongchen Wang, who passed away on July 9, 2013.

References

Abril, G., Bouillon, S., Darchambeau, F., Teodoru, C.R., Marwick, T.R., Tamooh, F., Ochieng Omengo, F., Geeraert, N., Deirmendjian, L., Polsenaere, P. and Borges, A.V., 2015. Technical Note: Large overestimation of pCO2 calculated from pH and alkalinity in acidic, organic-rich freshwaters. Biogeosciences, 12, 67-78.

Borges, A.V. and Gypens, N., 2010. Carbonate chemistry in the coastal zone responds more strongly to eutrophication than to ocean acidification. Limnol. Oceanogr., 55, 346-353.

Boucher, G., Clavier, J. and Garrigue, C., 1994. Oxygen and carbon dioxide fluxes at the water-sediment interface of a tropical lagoon. Mar. Ecol.-Prog. Ser., 107, 185-193.

Cai, W.-J., Hu, X., Huang, W.-J., Murrell, M.C., Lehrter, J.C., Lohrenz, S.E., Chou, W.-C., Zhai, W., Hollibaugh, J.T., Wang, Y., Zhao, P., Guo, X., Gundersen, K., Dai, M. and Gong., G.-C., 2011. Acidification of subsurface coastal waters enhanced by eutrophication. Nat. Geosci., 4, 766-770.

Canfield, D.E., Jorgensen, B.B., Fossing, H., Glud, R., Gundersen, J., Ramsing, N.B., Thamdrup, B., Hansen, J.W., Nielsen, L.P. and Hall, P.O.J., 1993. Pathways of organic carbon oxidation in three continental margin sediments. Mar. Geol., 113, 27-40.

Carter, B.R., Radich, J.A., Doyle, H.L. and Dickson, A.G., 2013. An automatic system for spectrophotometric seawater pH measurements. Limnol. Oceanogr.-Meth., 11, 16-27.

Checkley, D.M., Dickson, A.G., Takahashi, M., Radich, J.A., Eisenkolb, N. and Asch, R., 2009. Elevated CO_2 enhances otolith growth in young fish. Science, 324, 1683.

Chou, W.-C., Gong, G.-C., Sheu, D.D., Hung, C.-C. and Tseng, T.-F., 2009. Surface distributions of carbon chemistry parameters in the East China Sea in summer 2007. J. Geophys. Res., 114, C07026, doi:10.1029/2008JC005128.

Chou, W.-C., Gong, G.-C., Yang, C.-Y. and Chuang, K.-Y., 2016. A comparison between field and laboratory pH measurements for seawater on the East China Sea shelf. Limnol. Oceanogr.-Meth., n/a-n/a.

Chou, W.C., Gong, G.C., Cai, W.J. and Tseng, C.M., 2013a. Seasonality of CO2 in coastal oceans altered by increasing anthropogenic nutrient delivery from large rivers: evidence from the Changjiang–East China Sea system. Biogeosciences, 10, 3889-3899.

Chou, W.C., Gong, G.C., Hung, C.C. and Wu, Y.H., 2013b. Carbonate mineral saturation states in the East China Sea: present conditions and future scenarios. Biogeosciences, 10, 6453-6467.

Clayton, T.D. and Byrne, R.H., 1993. Spectrophotometric seawater pH measurements: total hydrogen ion concentration scale calibration of m-cresol purple and at-sea results. Deep-Sea Res. Pt. I, 40, 2115-2129.

Cooley, S.R., 2006. Dissolved inorganic carbon cycling in the offshore Amazon River plume and the western tropical North Atlantic ocean. PhD Thesis, University of Georgia, Athens, 298 pp.

Cripps, I.L., Munday, P.L. and McCormick, M.I., 2011. Ocean acidification affects prey detection by a predatory reef fish. PLoS ONE, 6, e22736.

Devol, A.H. and Hedges, J.I., 2001. Organic matter and nutrients in the mainstem Amazon River. In: M.E. McClain, R.L. Victoria and J.E. Richey (Editors), The Biogeochemistry of the Amazon Basin. Oxford University Press, pp. 275-306.

Dickson, A.G. and Millero, F.J., 1987. A comparison of the equilibrium constants for the dissociation of carbonic acid in seawater media. Deep Sea Res., 34, 1733-1743.

519 Dickson, A.G., Sabine, C.L. and Christian, J.R., 2007. Guide to Best Practices for Ocean CO_2
520 Measurements. PICES Special Publication 3.
521 Dickson, A.G., Wesolowski, D.J., Palmer, D.A. and Mesmer, R.E., 1990. Dissociation constant
522 of bisulfate ion in aqueous sodium chloride solutions to 250.degree.C. J. Phys. Chem.,
523 94, 7978-7985.
524 Doney, S.C., Fabry, V.J., Feely, R.A. and Kleypas, J.A., 2009. Ocean acidification: the other
525 CO_2 problem. Ann. Rev. Mar. Sci., 1, 169-192.
526 Duarte, C., Hendriks, I., Moore, T., Olsen, Y., Steckbauer, A., Ramajo, L., Carstensen, J.,
527 Trotter, J. and McCulloch, M., 2013. Is ocean acidification an open-ocean syndrome?
528 Understanding anthropogenic impacts on seawater pH. Estuar. Coast., 36, 221-236.
529 Egleston, E.S., Sabine, C.L. and Morel, F.o.M.M., 2010. Revelle revisited: Buffer factors that
530 quantify the response of ocean chemistry to changes in DIC and alkalinity. Global
531 Biogeochem. Cy., 24, doi:10.1029/2008GB003407.
532 Eldridge, P.M. and Morse, J.W., 2008. Origins and temporal scales of hypoxia on the Louisiana
533 shelf: Importance of benthic and sub-pycnocline water metabolism. Mar. Chem., 108,
534 159-171.
535 Fabry, V.J., 2008. Marine calcifiers in a high-CO_2 ocean. Science, 320, 1020-1022.
536 Feely, R.A., Alin, S.R., Newton, J., Sabine, C.L., Warner, M., Devol, A., Krembs, C. and Maloy,
537 C., 2010. The combined effects of ocean acidification, mixing, and respiration on pH and
538 carbonate saturation in an urbanized estuary. Estuar. Coast. Shelf S., 88, 442-449.
539 Feely, R.A., Sabine, C.L., Hernandez-Ayon, J.M., Ianson, D. and Hales, B., 2008. Evidence for
540 upwelling of corrosive "acidified" water onto the continental shelf. Science, 320, 1490-
541 1492.
542 Feely, R.A., Sabine, C.L., Lee, K., Berelson, W., Kleypas, J., Fabry, V.J. and Millero, F.J., 2004.
543 Impact of anthropogenic CO_2 on the $CaCO_3$ system in the oceans. Science, 305, 362-
544 366.
545 Fennel, K., 2010. The role of continental shelves in nitrogen and carbon cycling: Northwestern
546 North Atlantic case study. Ocean Sci., 6, 539-548.
547 Gattuso, J.-P., Epitalon, J.-M., Lavigne, H., Orr, J., Gentili, B., Hofmann, A., Proye, A., Soetaert,
548 K. and Rae, J., 2016. Seacarb: Seawater Carbonate Chemistry, http://CRAN.R-
549 project.org/package=seacarb.
550 Green, M.A. and Aller, R.C., 1998. Seasonal patterns of carbonate diagenesis in nearshore
551 terrigenous muds: Relation to spring phytoplankton bloom and temperature. J. Mar. Res.,
552 56, 1097-1123.
553 Guo, X., Cai, W.-J., Huang, W.-J., Wang, Y., Chen, F., Murrell, M.C., Lohrenz, S., Jiang, L.-Q.,
554 Dai, M., Hartmann, J. and Culp, R., 2012. CO2 dynamics and community metabolism in
555 the Mississippi River plume. Limnol. Oceanogr., 57, 1-17.
556 Hagens, M., Slomp, C.P., Meysman, F.J.R., Seitaj, D., Harlay, J., Borges, A.V. and Middelburg,
557 J.J., 2015. Biogeochemical processes and buffering capacity concurrently affect
558 acidification in a seasonally hypoxic coastal marine basin. Biogeosciences, 12, 1561-
559 1583.
560 Hu, X. and Cai, W.-J., 2011. The impact of denitrification on the atmospheric CO_2 uptake
561 potential of seawater. Mar. Chem., 127, 192-198.
562 Hu, X. and Cai, W.-J., 2013. Estuarine acidification and minimum buffer zone—A conceptual
563 study. Geophys. Res. Lett., 40, 5176-5181.

564 Huang, W.-J., Cai, W.-J., Wang, Y., Lohrenz, S.E. and Murrell, M.C., 2015. The carbon dioxide
565 (CO2) system on the Mississippi River–dominated continental shelf in the northern Gulf
566 of Mexico – I: Distribution and air-sea CO2 flux. J. Geophys. Res.-Oceans, 120, 1429-
567 1445.
568 Huang, W.J., Cai, W.J., Powell, R.T., Lohrenz, S.E., Wang, Y., Jiang, L.Q. and Hopkinson, C.S.,
569 2012. The stoichiometry of inorganic carbon and nutrient removal in the Mississippi
570 River plume and adjacent continental shelf. Biogeosciences, 9, 2781-2792.
571 IPCC, 2013. Climate Change 2013: The Physical Science Basis. Contribution of Working Group
572 I to the Fifth Assessment Report of the Intergovernmental Panel on Climate Change.
573 Cambridge University Press, Cambridge, United Kingdom and New York, NY, USA, .
574 Krumins, V., Gehlen, M., Arndt, S., Van Cappellen, P. and Regnier, P., 2013. Dissolved
575 inorganic carbon and alkalinity fluxes from coastal marine sediments: model estimates
576 for different shelf environments and sensitivity to global change. Biogeosciences, 10,
577 371-398.
578 Lehrter, J., Beddick, D., Devereux, R., Yates, D. and Murrell, M., 2012. Sediment-water fluxes
579 of dissolved inorganic carbon, O, nutrients, and N2 from the hypoxic region of the
580 Louisiana continental shelf. Biogeochemistry, 109, 233-252.
581 Liu, X., Patsavas, M.C. and Byrne, R.H., 2011. Purification and characterization of meta-cresol
582 purple for spectrophotometric seawater pH measurements. Environ. Sci. Technol., 45,
583 4862-4868.
584 Lueker, T.J., Dickson, A.G. and Keeling, C.D., 2000. Ocean pCO_2 calculated from dissolved
585 inorganic carbon, alkalinity, and equations for K_1 and K_2: validation based on laboratory
586 measurements of CO_2 in gas and seawater at equilibrium. Mar. Chem., 70, 105-119.
587 McCarthy, M.J., Carini, S.A., Liu, Z., Ostrom, N.E. and Gardner, W.S., 2013. Oxygen
588 consumption in the water column and sediments of the northern Gulf of Mexico hypoxic
589 zone. Estuar. Coast. Shelf S., 123, 46-53.
590 Mehrbach, C., Culberson, C.H., Hawley, J.E. and Pytkowicz, R.M., 1973. Measurement of the
591 apparent dissociation constants of carbonic acid in seawater at atmospheric pressure.
592 Limnol. Oceanogr., 18, 897-907.
593 Millero, F.J., 2010. Carbonate constants for estuarine waters. Mar. Freshwater Res., 61, 139-
594 142.
595 Millero, F.J., Lee, K. and Roche, M., 1998. Distribution of alkalinity in the surface waters of the
596 major oceans. Mar. Chem., 60, 111-130.
597 Millero, F.J., Pierrot, D., Lee, K., Wanninkhof, R., Feely, R., Sabine, C.L., Key, R.M. and
598 Takahashi, T., 2002. Dissociation constants for carbonic acid determined from field
599 measurements. Deep-Sea Res. Pt. I, 49, 1705-1723.
600 Mosley, L.M., Husheer, S.L.G. and Hunter, K.A., 2004. Spectrophotometric pH measurement in
601 estuaries using thymol blue and m-cresol purple. Mar. Chem., 91, 175-186.
602 Mucci, A., Starr, M., Gilbert, D. and Sundby, B., 2011. Acidification of lower St. Lawrence
603 Estuary bottom waters. Atmos.-Ocean, 49, 206-218.
604 Murrell, M. and Lehrter, J., 2011. Sediment and lower water column oxygen consumption in the
605 seasonally hypoxic region of the Louisiana Continental Shelf. Estuar. Coast., 34, 912-
606 924.
607 Nixon, S., Oczkowski, A., Pilson, M.Q., Fields, L., Oviatt, C. and Hunt, C., 2015. On the
608 response of pH to inorganic nutrient enrichment in well-mixed coastal marine waters.
609 Estuar. Coast., 38, 232-241.

610 Orr, J.C., Fabry, V.J., Aumont, O., Bopp, L., Doney, S.C., Feely, R.A., Gnanadesikan, A.,
611 Gruber, N., Ishida, A., Joos, F., Key, R.M., Lindsay, K., Maier-Reimer, E., Matear, R.,
612 Monfray, P., Mouchet, A., Najjar, R.G., Plattner, G.-K., Rodgers, K.B., Sabine, C.L.,
613 Sarmiento, J.L., Schlitzer, R., Slater, R.D., Totterdell, I.J., Weirig, M.-F., Yamanaka, Y.
614 and Yool, A., 2005. Anthropogenic ocean acidification over the twenty-first century and
615 its impact on calcifying organisms. Nature, 437, 681-686.
616 Pasch, R.J., 2010. Tropical cyclone report Hurricane Alex (AL012010) 25 June–2 July 2010
617 National Hurricane Center pp. 19.
618 Patsavas, M.C., Byrne, R.H., Wanninkhof, R., Feely, R.A. and Cai, W.-J., 2015. Internal
619 consistency of marine carbonate system measurements and assessments of aragonite
620 saturation state: insights from two U.S. coastal cruises. Mar. Chem., 176, 9-20.
621 Pawlowicz, R., 2015. The absolute salinity of seawater diluted by riverwater. Deep-Sea Res. Pt.
622 I, 101, 71-79.
623 Pierrot, D., Lewis, E. and Wallace, D.W.R., 2006. MS Excel Program Developed for CO2
624 System Calculations. ORNL/CDIAC-105a. Carbon Dioxide Information Analysis Center,
625 Oak Ridge National Laboratory, U.S. Department of Energy, Oak Ridge, Tennessee. .
626 Rabalais, N., Turner, R.E., Dortch, Q., Justic, D., Bierman, V. and Wiseman, W., 2002. Nutrient-
627 enhanced productivity in the northern Gulf of Mexico: past, present and future.
628 Hydrobiologia, 475-476, 39-63.
629 Rabalais, N.N., DÃaz, R.J., Levin, L.A., Turner, R.E., Gilbert, D. and Zhang, J., 2010. Dynamics
630 and distribution of natural and human-caused hypoxia. Biogeosciences, 7, 585-619.
631 Rabalais, N.N., Turner, R.E., Sen Gupta, B.K., Boesch, D.F., Chapman, P. and Murrell, M.C.,
632 2007. Hypoxia in the northern Gulf of Mexico: Does the science support the plan to
633 reduce, mitigate, and control hypoxia? Estuar. Coast., 30, 753-772.
634 Rabalais, N.N., Turner, R.E. and Wiseman, W.J., 2001. Hypoxia in the Gulf of Mexico. J.
635 Environ. Qual., 30, 320-329.
636 Raymond, P.A. and Cole, J.J., 2003. Increase in the export of alkalinity from North America's
637 largest river. Science, 371, 88-91.
638 Raymond, P.A., Oh, N.-H., Turner, R.E. and Broussard, W., 2008. Anthropogenically enhanced
639 fluxes of water and carbon from the Mississippi River. Nature, 451, 449-452.
640 Reisdorph, S.C. and Mathis, J.T., 2014. The dynamic controls on carbonate mineral saturation
641 states and ocean acidification in a glacially dominated estuary. Estuar. Coast. Shelf S.,
642 144, 8-18.
643 Rowe, G.T., Kaegi, M.E.C., Morse, J.W., Boland, G.S. and Briones, E.G.E., 2002. Sediment
644 community metabolism associated with continental shelf hypoxia, Northern Gulf of
645 Mexico. Estuaries, 25, 1097-1106.
646 Salisbury, J., Green, M., Hunt, C. and Campbell, J., 2008. Coastal acidification by rivers: a threat
647 to shellfish? EOS, 89, 513-514.
648 Sunda, W.G. and Cai, W.-J., 2012. Eutrophication induced CO2-acidification of subsurface
649 coastal waters: interactive effects of temperature, salinity, and atmospheric pCO2.
650 Environ. Sci. Technol., 46, 10651–10659.
651 Tian, H., Yang, Q., Najjar, R.G., Ren, W., Friedrichs, M.A.M., Hopkinson, C.S. and Pan, S.,
652 2015. Anthropogenic and climatic influences on carbon fluxes from eastern North
653 America to the Atlantic Ocean: A process-based modeling study. J. Geophys. Res.-
654 Biogeo., 120, 2014JG002760.

Turner, R.E., Rabalais, N.N. and Justic, D., 2006. Predicting summer hypoxia in the northern Gulf of Mexico: Riverine N, P, and Si loading. Mar. Pollut. Bull., 52, 139-148.

Uppström, L.R., 1974. The boron/chlorinity ratio of deep-sea water from the Pacific Ocean. Deep-Sea Res.: Oceanogr. Abstr., 21, 161-162.

USEPA, 1993. Methods of chemical analysis of water and wastes. Environmental Monitoring Support Laboratory, Cincinnati.

Waldbusser, G.G., Brunner, E.L., Haley, B.A., Hales, B., Langdon, C.J. and Prahl, F.G., 2013. A developmental and energetic basis linking larval oyster shell formation to acidification sensitivity. Geophys. Res. Lett., 40, 1–6.

Wallace, R.B., Baumann, H., Grear, J.S., Aller, R.C. and Gobler, C.J., 2014. Coastal ocean acidification: The other eutrophication problem. Estuar. Coast. Shelf S., 148, 1-13.

Wang, P. and Roberts, T.M., 2013. Distribution of surficial and buried oil contaminants across sandy beaches along NW Florida and Alabama coasts following the Deepwater Horizon oil spill in 2010. J. Coastal Res., 144-155.

Wanninkhof, R., Barbero, L., Byrne, R., Cai, W.-J., Huang, W.-J., Zhang, J.-Z., Baringer, M. and Langdon, C., 2015. Ocean acidification along the Gulf Coast and East Coast of the USA. Cont. Shelf. Res., 98, 54-71.

Weiss, R.F., 1974. Carbon dioxide in water and seawater: the solubility of a non-ideal gas. Mar. Chem., 2, 203-215.

Williams, R.G. and Follows, M.J., 2011. Ocean Dynamics and the Carbon Cycle. Cambridge University Press, New York.

Xue, J., Cai, W.-J., Hu, X., Huang, W.-J., Lohrenz, S.E. and Gundersen, K., 2015. Temporal variation and stoichiometric ratios of organic matter remineralization in bottom waters of the northern Gulf of Mexico during late spring and summer. J. Geophys. Res.-Oceans, DOI: 10.1002/2015JC011453.

Yang, B., Byrne, R.H. and Lindemuth, M., 2015. Contributions of organic alkalinity to total alkalinity in coastal waters: A spectrophotometric approach. Mar. Chem., 176, 199-207.

Yao, W., Liu, X. and Byrne, R.H., 2007. Impurities in indicators used for spectrophotometric seawater pH measurements: Assessment and remedies. Mar. Chem., 107, 167-172.

Zhai, W., Dai, M. and Guo, X., 2007. Carbonate system and CO_2 degassing fluxes in the inner estuary of Changjiang (Yangtze) River, China. Mar. Chem., 107, 342-356.

688 **Figure captions**

689 Figure 1. Salinity (a, e), $\Omega_{aragonite}$ (b, f), pH (on total scale, c, g), and dissolved oxygen (d, h) in
690 surface and bottom waters of the nGoM during the Shelfwide Hypoxia Cruise (July 25-31,
691 2010). Crosses (+) represent sampling locations. The Atchafalaya and Mississippi deltas are
692 marked with A and M, respectively (panel a).

693 Figure 2. Distribution of buffer factor $ß_{DIC}$ in surface and bottom waters.

694 Figure 3. Surface and bottom pH (total scale) in nGoM waters. Closed circles represent surface
695 water, and closed triangles represent bottom water. The solid line is a simulated average river-
696 ocean mixing curve based on a combination of four mixing scenarios (high vs. low river TA ×
697 high vs. low seawater temperature, the same also applies to the calculations of the other two
698 reaction/mixing curves). The dotted line is based on simulations that all riverine nitrate+nitrite is
699 consumed. The dashed line represents complete anoxia starting from saturated DO
700 concentrations along the entire salinity range. The shaded areas represent one standard deviation
701 of each set of four simulations for the conservative mixing, respiration, and photosynthesis,
702 respectively.

703 Figure 4. Distributions of buffer factor $ß_{DIC}$ in surface and bottom waters. Closed circles
704 represent surface water, and closed triangles represent bottom water. The simulation curves
705 represent four mixing scenarios that account for river end-member TA and seawater temperature
706 (see caption for Fig. 3 and text for details).

707 Figure 5. Spatial distribution of pCO_2 in surface (a) and bottom (b) waters.

708 Figure 6. pH-DO (a) and DIC-DO (b) relationships. All data were collected in bottom waters
709 with salinity >32 and water depth >12 m. The solid triangles are data collected from this study,
710 and the open circles represent data reported in Cai et al. (2011). The solid black and gray lines

represent aerobic respiration induced pH_T (a) and DIC (b) changes from two high DO water samples at the high DO 'core' between 92.0°W and 92.5°W (see Fig. 2). Starting conditions for these two samples were: S_1=35.5, T_1=28.80°C, P_1 = 28.25 dbar, DO_1 = 169.2 µmol kg^{-1}, DIC_1 = 2065.6 µmol kg-1, TA_1=2394.7 µmol kg-1, $[PO_4^{3-}]_1$ = 1.1 µmol kg^{-1}, $[H_2SiO_3]_2$ = 10.2 µmol kg^{-1}, and S_2=35.5, T_2=23.56°C, P_2=36.47 dbar, DO_2 = 172.1 µmol kg^{-1}, DIC_2 = 2105.0 µmol kg-1, TA_2=2397.3 µmol kg^{-1}, $[PO_4^{3-}]_2$ = 0.8 µmol kg^{-1}, $[H_2SiO_3]_2$ = 7.0 µmol kg^{-1}. The dashed lines account for benthic DIC contributions with the benthic flux values from Rowe et al. (2002) for each starting DO concentration.

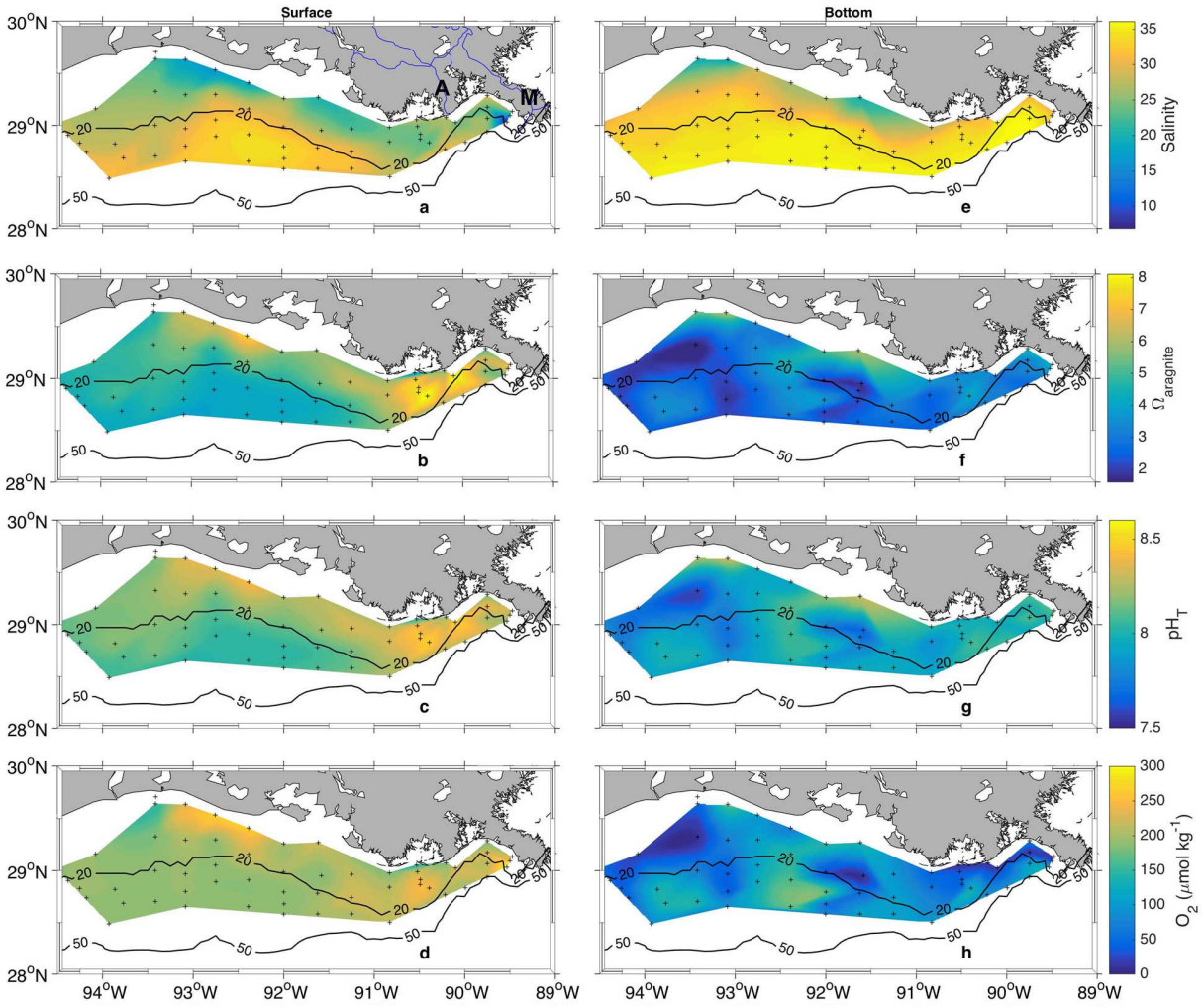

719

720

721 Figure 1

722

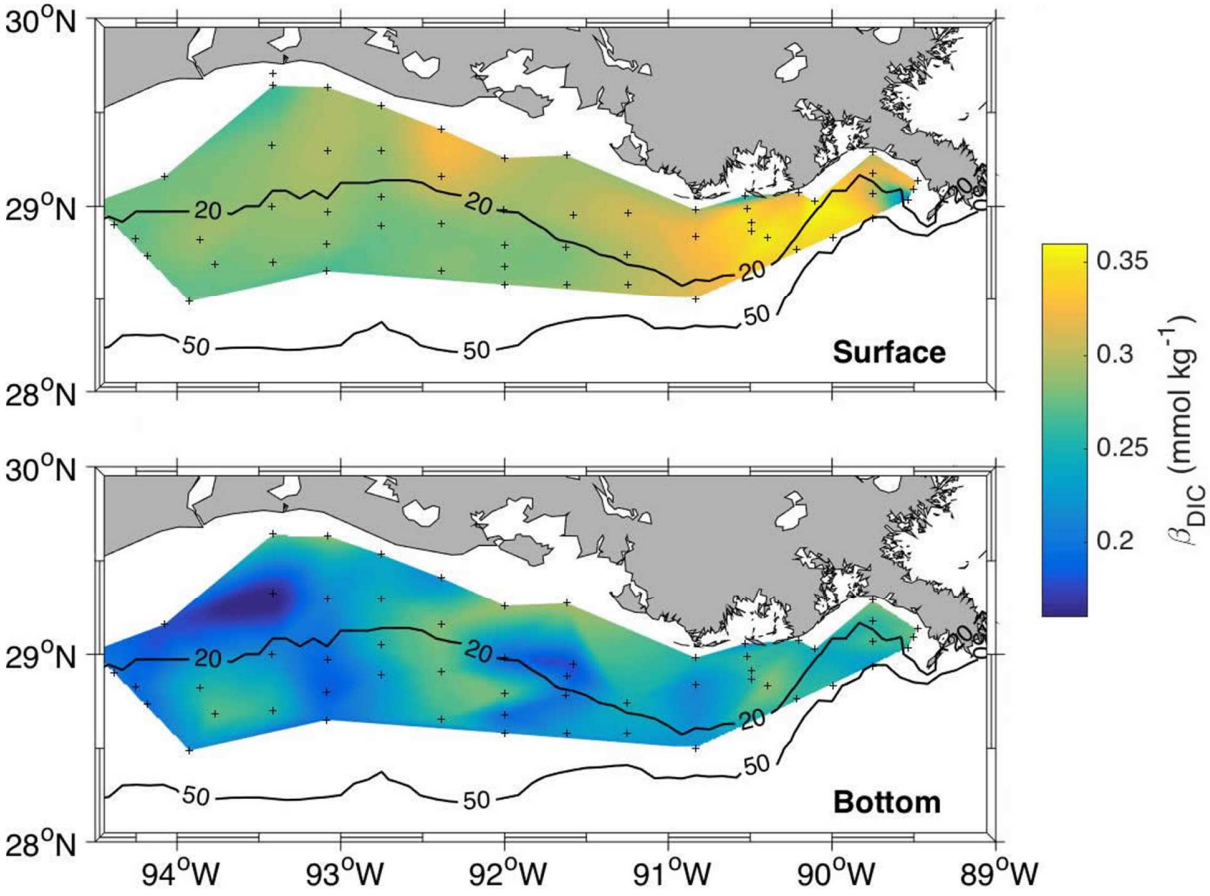

723

724

725 Figure 2

726

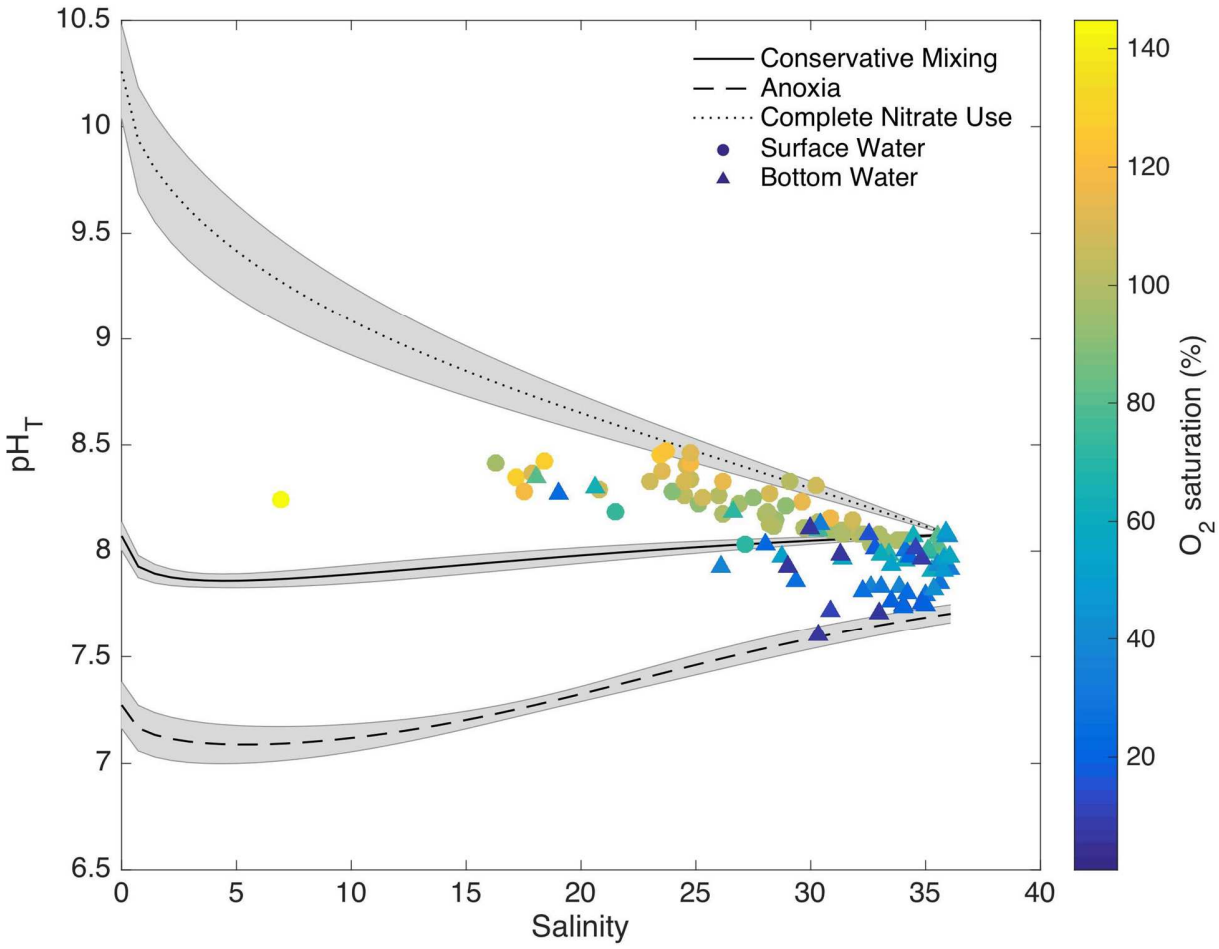

727

728 Figure 3.

729

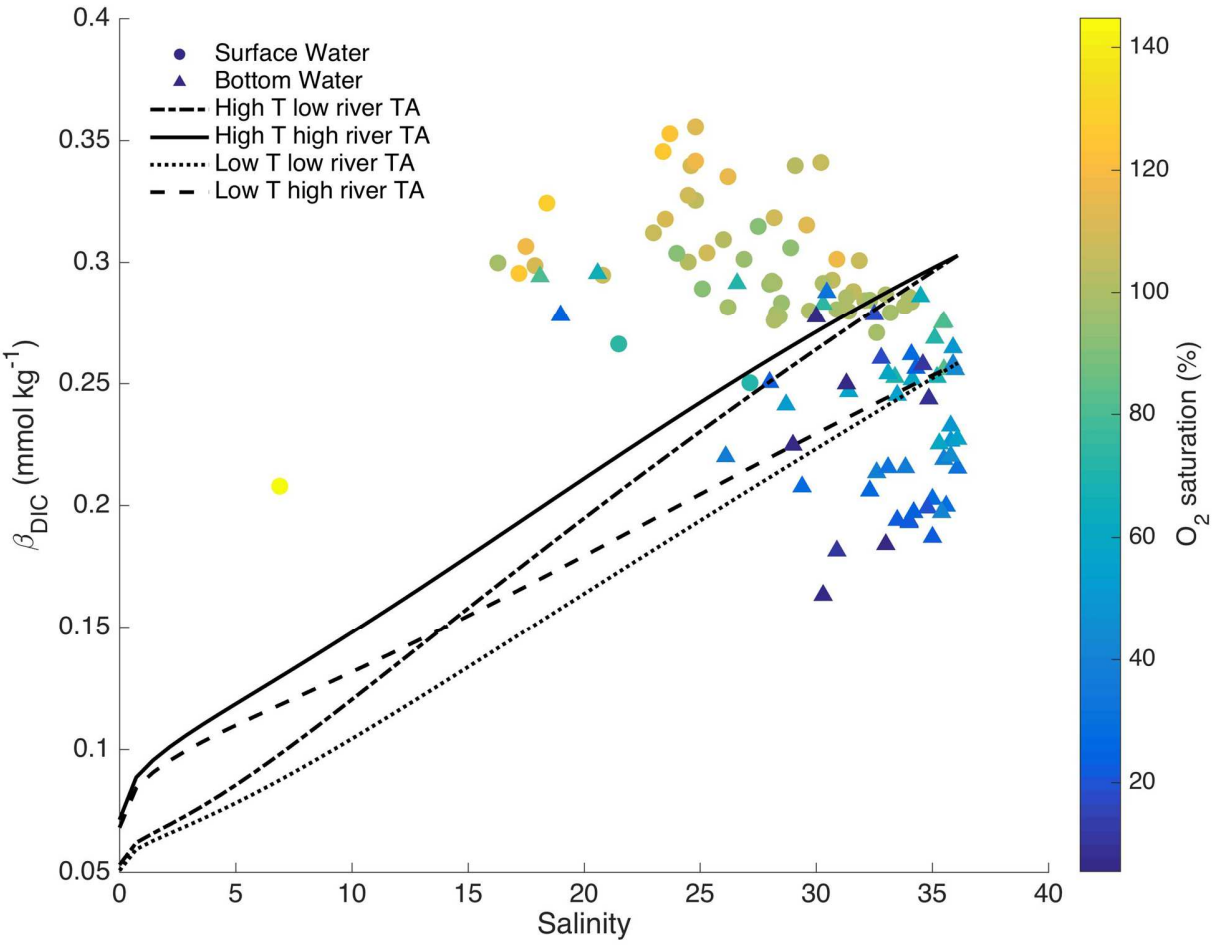
Surface Water
Bottom Water
High T low river TA
High T high river TA
Low T low river TA
Low T high river TA
β_{DIC} (mmol kg^{-1})
Salinity
O_2 saturation (%)
0.4
0.35
0.3
0.25
0.2
0.15
0.1
0.05
0
5
10
15
20
25
30
35
40
140
120
100
80
60
40
20

730

731 Fig. 4

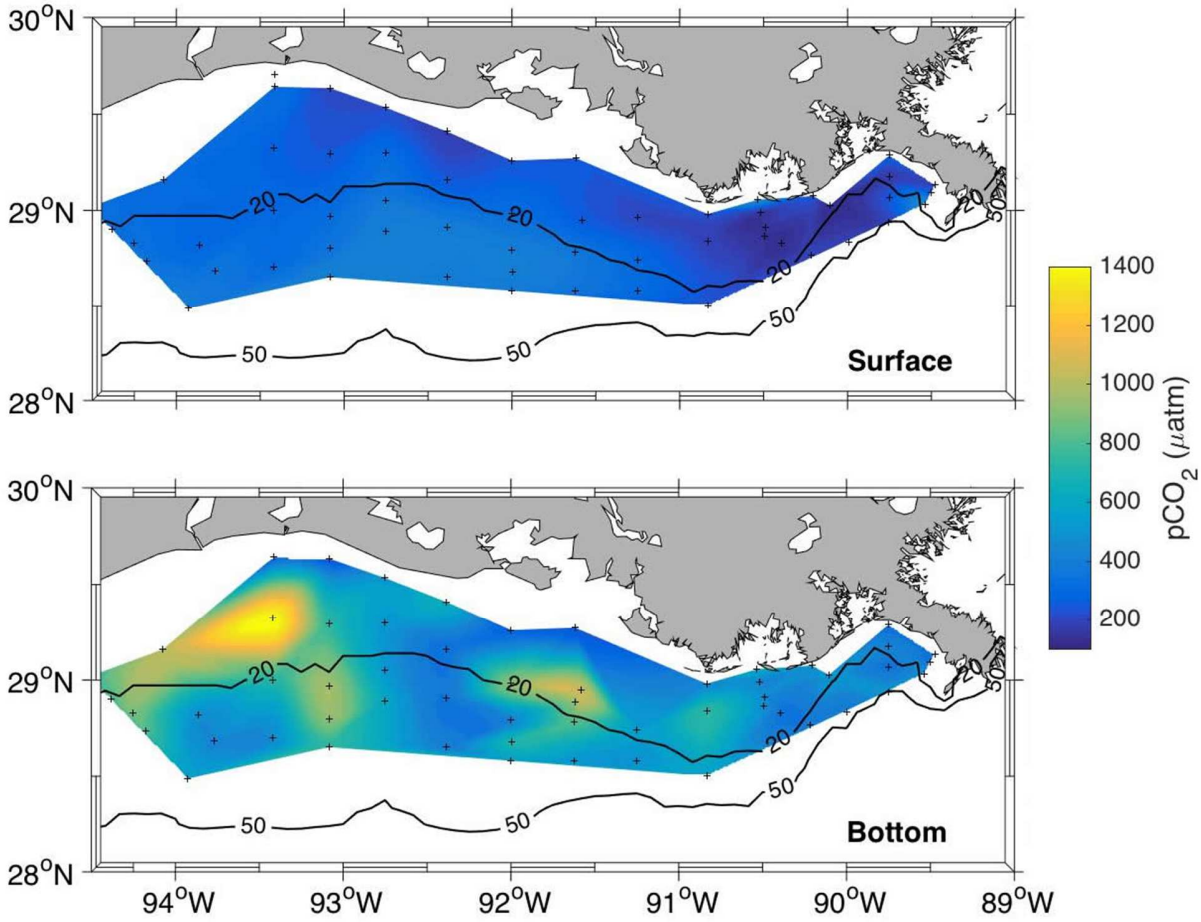

732

733 Fig. 5

734

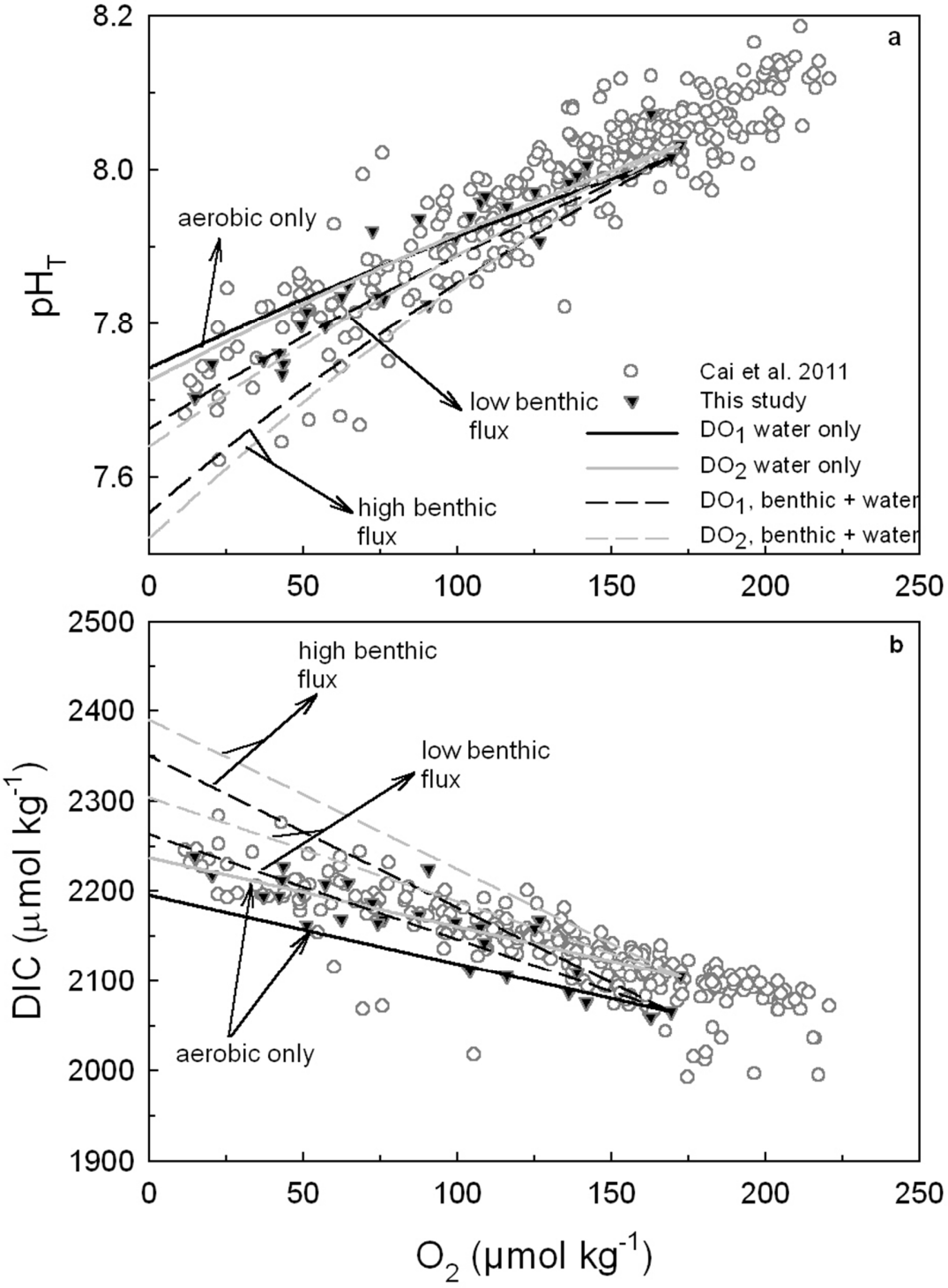

735

736

737 Fig. 6